A data-driven framework for landslide size space-time modelling

Zhice Fang[1,2], Yi Wang[1,*], Cees van Westen[2], Luigi Lombardo[2]

[1] Institute of Geophysics and Geomatics, China University of Geosciences, Wuhan 430074, China

[2] University of Twente, Faculty of Geo-Information Science and Earth Observation (ITC), PO Box 217, Enschede, AE 7500, Netherlands

[*]Correspondence Author: Yi Wang (cug.yi.wang@gmail.com)

Abstract

Landslide susceptibility assessment using data-driven models has predominantly focused on predicting where landslides may occur and not on how large they might be. The spatio-temporal evaluation of landslide susceptibility has only recently been addressed, as a basis for predicting where and when landslides might occur. The present study combines these new developments by proposing a data-driven model capable of estimating how large landslides may be, for the Taiwan territory in a fourteen-year time window. To solve this task, our model assumes that landslide sizes follow a Log-Gaussian probability distribution in space and time. Spatially the area is subdivided into 46074 slope units, with 14 annual timesteps from 2004 to 2018. Based on this subdivision, the model we implemented regressed landslide sizes against a covariate set that includes temporally static and dynamic properties. In the validation of our model, we nested a wide range of cross-validation (CV) procedures, includes a randomized 10fold-CV, a spatially constrained CV, a temporal leave-one-year-out CV, and a spatio-temporal CV. The final performance was described both numerically as

well as in map forms. Overall, our space-time model achieves interpretable and satisfactory results. With the availability of more complete landslide inventories, both temporally and spatially, we envision that spatio-temporal landslide size prediction will become the next challenge for geomorphologists to finally address a fundamental component of the landslide hazard definition. And, because of its spatio-temporal nature, we also envision that it may lead to simulation studies for varying climate scenarios.

Keywords: dynamic landslide area prediction; space-time modelling; slope unit; spatio-temporal cross-validation

1. Introduction

Landslides are a common natural hazard in many mountainous landscapes worldwide, and pose a serious threat to human lives and properties (Rossi et al., 2019; Merghadi et al., 2020). Therefore, accurate prediction of landslide location and size is a crucial requirement for reliable hazard and subsequent risk assessment. The most commonly accepted definition of landslide hazard requires the estimation of three aspects: i) the probability of occurrence at a given location, ii) within a specified period, and iii) with a given magnitude (Varnes, 1984; Guzzetti et al., 1999; Guzzetti et al., 2005). This definition essentially addresses three main questions that a decision maker requires to implement any risk mitigation strategy: “where”, “how frequent”, and “how large” landslides are likely to occur in a certain area. This definition was later improved by Corominas et al. (2014) as they introduced the landslide intensity concept to measure the spatial variation in the threat level that landslides may carry across a landscape. However, the intensity that Corominas and co-authors mainly considered consists of dynamic spatially distributed characteristics such as velocity, impact pressure or kinematic energy, which are derived using physically-based models. Due to the heterogeneity of the landscape, the parameters for these models are virtually impossible to collect over larger areas, which is the reason why recent efforts have been made towards expressing landslide intensity over larger areas in terms of counts (Lombardo et al., 2018) or sizes (Lombardo et al., 2021) as a basis for data-driven modelling. These publications represent two examples of a long list of data-driven studies in the context of landslide prediction, which were largely dedicated to purely predicting occurrence locations (or susceptibility), and only recently they have branched out towards other landslide characteristics. Specifically, data-driven susceptibility models were initially framed in a bivariate statistical structure (e.g., Van Westen et al., 2003; Nandi and Shakoor, 2010), and this essentially remained the case until they were superseded by their multivariate statistics counterpart (e.g., Chung et al., 1995; Atkinson and Massari, 1998). Only recent years have witnessed the spread of machine learning (e.g., Merghadi et al., 2020) and deep learning (e.g., Fang et al., 2021; Aguilera et al., 2022) architectures with improved predicting performance they ensure. These models have mostly been used purely in space, with very few applications to the space-time context (Lombardo et al., 2020), aside from empirical rainfall thresholds (Jaiswal et al., 2010; Nefeslioglu and Gorum, 2020) or coseismic near-real-time predictions (Nowicki Jessee et al., 2018).

Specifically for statistical studies, a common assumption is the choice of a suitable distribution reflecting the data on landslides. For this reason, susceptibility models assume a Bernoulli probability distribution (Steger et al., 2016; Steger et al., 2017), whereas intensity models based on landslide counts assume the Poisson probability distribution (Lombardo et al., 2019; Opitz et al., 2022). When it comes to model landslide area, the choice is not straightforward. In fact, it is common that a landslide area distribution is quite heavily tailed. In other words, the vast majority of inventories includes a predominant number of small landslides and only few extremely large ones, which is common in response to major triggering events, such as rainfall (Jones et al., 2021; Emberson et al., 2022) or earthquakes (Zhang et al., 2019; Tanyaş et al., 2022). This is the reason that has led Malamud et al. (2004) to propose the Inverse Gamma distribution as a universal empirical size model, which leads to a series of studies on landslide Frequency Area Distribution (FAD; Tanyaş et al., 2018). However, one weakness of the FAD approach is that it neglects the spatial distribution of the landslides it considers, something that has been recently accounted for in a few articles on the subject. Specifically, Lombardo et al. (2021) and Moreno et al. (2022) were the first to propose a Log-Gaussian model able to estimate the expected planimetric extent of landslides over a given landscape. However, their model lacked the ability to inform whether any given slope will be unstable. For this reason, Aguilera et al. (2022) and Bryce et al. (2022) extended this framework by building a joint landslide susceptibility and area prediction model. But even in these cases, one main issue still persisted, for they produced temporally stationary estimates of landslide extents. By leaving the temporal dimension unexplored, most studies neglected a crucial requirement of both hazard definitions proposed by Guzzetti et al. (1999) and Corominas et al. (2014), and even reported in the international guidelines for landslide risk (Fell et al., 2008). Also, such stationary models may not be valid over large areas and in the context of rapid climate change, because global warming can influence landslide activity, abundance, and frequency (Gariano and Guzzetti, 2016). Therefore, an important research gap to be addressed relates to how these purely spatial size models can be reliably extended over time.

One way to do so is based on physically-based modelling (Park et al., 2019; Van den Bout et al., 2021). However, the unavailability of required geotechnical parameters mostly constrains their applicability to individual slopes or small catchment analyses. Data-driven approaches can by-pass the geotechnical requirements as long as a reliable multi-temporal landslide inventory is available (Guzzetti et al., 2012), together with a set of static and dynamic explanatory variables (Wang et al., 2021) capable of explaining landslide size distribution in space and time. Based on these considerations, we propose a space-time landslide size model to estimate the planimetric landslide area in any given mapping and temporal unit. Specifically, we present the implementation of a Log-Gaussian generalized additive model (GAM), which assumes that the landslide size follows a log-Gaussian distribution in the space-time domain. The spatio-temporal characteristics of landslide size are captured by incorporating a set of static and dynamic factors. The same model is constrained to treat mapping units that are close in space to behave more similarly compared to those that are far away, and the same is valid in time.

We tested this model with a dataset of the main island of Taiwan for the period from 2004 to 2018, during which tropical cyclones triggered many landslides. This present study aims at estimating probabilistically "how frequent" and "how large" landslides are expected within mapping units. We consider this a step towards a new generation of probabilistic landslide hazard assessment, beyond what is currently available in the literature.

2. Study area and data overview

2.1. Study area

We implemented the space-time landslide size modelling in the main island of Taiwan (**Fig. 1**), where extends over a total of 35,808 km^2. Taiwan is frequently affected by landslides triggered by typhoons and/or earthquakes, a unique condition owed to its geographical location in the Pacific Ring of Fire and in the path of tropical cyclones. For example, the 1999 Chi-Chi earthquake triggered more than 10,000 landslides in central Taiwan, with a total sliding area of exceeding 100 km^2 (Hung, 2000). Typhoon Morakot in 2009 brought an accumulated rainfall of 3059 mm and resulted in more than 22,705 landslides covering an total area of 274 km^2 (Lin et al., 2011).

2.2. Landslide inventory

The Forestry Bureau of Taiwan has produced a yearly landslide inventory for the whole Taiwan from 2004 to 2018 (https://data.gov.tw/). The expert landslide and shaded area delineation system (ELSADS) was used to produce each landslide inventory map (Lin et al., 2013; Liu, 2015). The ELSADS system first uses the principal component analysis, NDVI and normalized green red difference indices (NGRDI) to exclude dark areas and vegetated areas. Then, it overlays non-vegetated areas with the standard-false-color image and DTM in a 3D view, and combines multi-source information (e.g., earlier images, base map, and land use map) to detect landslide areas. These manipulations could reduce negative influence from shaded area, cultivated land, roads, houses, and riverbeds. The inventory is based on the interpretation of Formosat-2 satellite images (2 m spatial resolution) collected between January and July for each year, and validated using aerial images (25 cm spatial resolution). Several scientists have used this inventory for different applications. For example, Lin et al. (2017) analyzed the evolution of landslides across Taiwan using a statistical technique based on the same multi-temporal landslide inventory as our study. Chen et al. (2019a) analyzed the effects of climate changes on landslide activities in northern Taiwan. Other applications of this multi-temporal inventory include landslide detection (Chen et al., 2019b) and landslide susceptibility modelling in Taiwan (Chang et al., 2015; Chang et al., 2019).

These annual landslide maps do not distinguish new landslides that occurred in a specific year from those that already existed. Therefore, to isolate the contribution of new occurrences and/or reactivated failures, we calculated the difference of two subsequent yearly inventories to derive landslide expansion areas for each year under consideration. For example, if we calculate the landslides for the year 2005 minus those of 2004, then positive values imply new failed surfaces. Finally, we obtained 14 new landslide maps (**Fig. 1**), and each represents the landslide expansion areas from the first of August to the last day of July of the next year. We aggregated the landslide planimetric area in each slope unit and considered it as the target variable of the model.

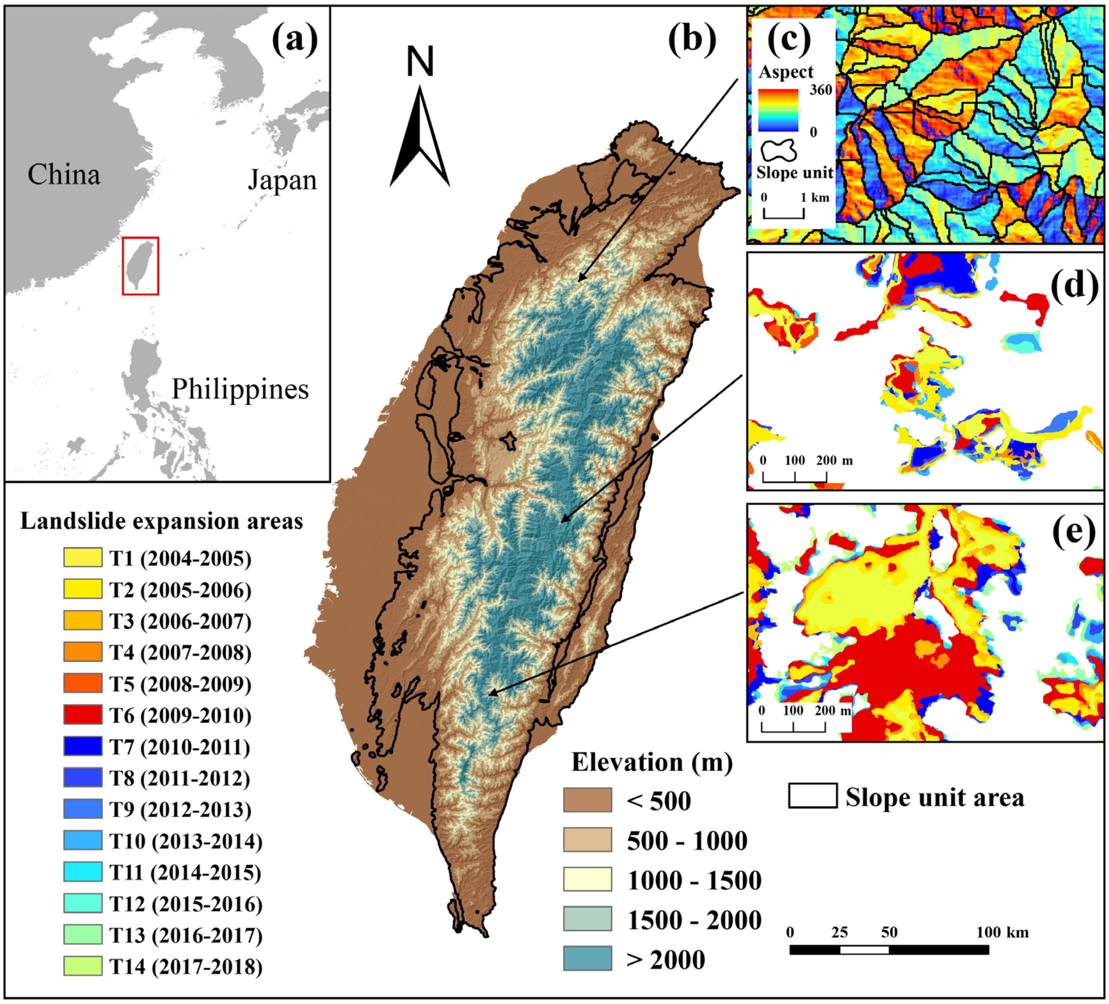

Fig. 1 (a) Location of the study area; (b) elevation distribution of Taiwan island; (c) a sub-region showing the slope units partition, and (d, f) spatial distribution of landslides in two sub-regions from 2004 to 2018. Landslides in each time period denotes the expansion area from August 1st of the current

year to July 31st of the next year.

2.3. Explanatory factors

In the context of a space-time modelling implemented, some landslide related factors can be simplified as constant properties, whereas others may exhibit some degrees of temporal variation on a daily, seasonal or yearly basis. For this reason, we prepared a set of static and dynamic factors to build our space-time model. Specifically, we derived eight static terrain attributes from a 30 m NASA DEM product (accessible at https://earthdata.nasa.gov/), which is a re-release of the SRTM DEM based on an improved calibration and additional void-filling. Five topographic factors calculated based on DEM data have widely been employed (e.g., Lee et al., 2008; Cama et al., 2017): slope, plan curvature, profile curvature, northness, and eastness. In the present study, we also obtained three relief-related factors (intensity, range, and variance) derived from DEM data to represent the gravitational potential energy across the terrain (Stepinski and Jasiewicz, 2011). The relief intensity denotes the average difference between the elevation of a grid-cell and those included in a neighborhood. The relief range denotes the difference between max and min elevations within the cell extend. The relief is the variability of the elevations values within the cell extend. Notably, the hillslope relief has appeared in a number of studies dedicated to landslide size (Medwedeff et al., 2020), and has proven to be a dominant covariate in landslide size predictive modelling (Lombardo et al., 2021). We also considered the variation in lithological conditions, expressed through 15 classes derived from a 1:250,000 scale geological map (see Appendix A for the descriptions). We also generated the Euclidean distance to faults, derived from a 1: 50,000 scale fault map. The above two geological factors can be accessed via the Central Geological Survey of Taiwan (https://www.geologycloud.tw/). Furthermore, we used slope units derived from the

DEM as our basic terrain unit. The slope unit area is selected to describe the geometric properties of the terrain unit. We also considered the dual interaction between longitude and latitude of each mapping unit centroid to represent the spatial structure of the Taiwan landscape. All the above factors belong to the stationary set of predictors we selected for our space-time modelling procedure.

As for the dynamic factors, we opted to include rainfall, normalized difference vegetation index (NDVI), and a yearly function of timesteps between subsequent inventories. The maximum daily rainfall is considered as a dynamic climate factor in the yearly space-time landslide size model. We collected the rainfall estimates from 188 meteorological stations and interpolated the yearly daily maximum rainfall via a cokriging routine, which used elevation as a parameter to represent the orographic effect on the precipitation patterns. To describe the effect of vegetation, we calculated the yearly maximum NDVI based on Landsat-7 images (30 m spatial resolution) via the Google Earth Engine platform. Ultimately, the temporal effect on landslide sizes was brought into the model as a function of the timesteps between subsequent landslide occurrences, that is, we labeled each slope unit with an ID to indicate which yearly landslide inventory it belongs to.

3. Methodology

3.1. Mapping and temporal units

Determining appropriate mapping and temporal units is important for any space-time modelling. To geographically partition the landscape, we generated slope units (SUs) as our reference terrain units for they well reflect the slope morphodynamics (Guzzetti et al., 1999), and they cover the landscape units between sub-catchment divides and streams, making them particularly suitable for landslide modeling (Carrara, 1988). Since our study focuses on the whole main island of Taiwan, which has extensive flat areas along the coasts, we used the r.geomorphon module (Jasiewicz and Stepinski, 2013) available in GRASS GIS to outline flat areas. In a subsequent step, we excluded them from the analysis performed by the r.slopeunits software (Alvioli et al., 2016), a tool to automatically delineate SUs on the basis of an aspect-homogeneity criterion. This resulted in 46,074 polygons with a mean SU area of 589,844 m^2 and a standard deviation of 395,973 m^2. As for the temporal dimension, we chose a temporal unit of one year (from August 1st of the current year to July 31st of the next year). The resulting space-time domain therefore featured 645,036 units, made of 46,074 SUs and repeated over the 14 temporal units.

For the covariates listed in Section 2.3, each of these units need to be assigned with a covariate value, (see **Table 1**). The spatial extent of the SUs requires an upscaling step. In fact, a large number of grid-cells can be hosted in a SU, from which a distribution of potential values can be derived. Thus, to account for the associated intra-SU variability, we derived two statistical moments in the form of the mean and standard deviation for all terrain attributes, distance to faults, and NDVI. As for the lithological characterization of each SU, we extracted the class with the largest areal extent as a representative for the whole SU. Because the maximum daily rainfall has a more even distribution over the SUs, we only extracted the mean precipitation value per SU, and not the standard deviation.

Unlike landslide susceptibility modelling where the focus is given to landslide presence/absence data, our size model requires information on the planimetric landslide extent per SU. To estimate this extent and later use it as a response variable of our model, we computed the sum of all landslide areas falling within each SU and converted the resulting heavy-tailed distribution by using the logarithmic transformation. From this, we extracted the positive part of the landslide area distribution (removing the zeros or those units with no landslides) giving rise to a spatio-temporal domain consisting of 119,545 SUs (with a total landslide area of 1732.55 km^2).

Table 1 Summary of covariates used in the study.

Type	Covariates	Description
Static	Mean slope	Mean and standard deviation (SD) of morphological factors in each slope unit
	Slope-SD	
	Mean plan curvature	
	PlanCurv-SD	
	Mean profile curvature	
	ProfileCurv-SD	
	Mean northness	
	North-SD	
	Mean eastness	
	East-SD	
	Mean relief intensity	
	ReliefInt-SD	
	Mean relief range	
	ReliefRan-SD	
	Mean relief variance	
	ReliefVar-SD	
	Mean distance to faults	Mean of distance to faults in each slope unit
	FaultDis-SD	SD of distance to faults in each slope unit
	Lithology	Majority class in each slope unit.
	Slope unit area	Area of each slope unit
	Spatial location	longitude and latitude of the centroid in each SU
Dynamic	Maximum daily rainfall	Mean of rainfall per year in each slope unit
	Mean NDVI	Mean of NDVI per year in each slope unit
	NDVI-SD	SD of NDVI per year in each slope unit
	Time period	Time period ID for each slope unit

3.2. Generalized additive model

A generalized additive model (GAM) can estimate linear and nonlinear effects between explanatory and target variables (Goetz et al., 2011). As a result, these models can provide satisfying performance while maintaining flexibility and interpretability. GAMs have been successfully used in a number of spatially-explicit models for landslide occurrences, dedicated to landslide susceptibility (e.g., Steger et al., 2016; Titti et al., 2021) and intensity assessments (e.g., Lombardo et al., 2019). The same GAM framework has recently been used by Lombardo et al. (2021) _ENREF_32through assuming that landslide planimetric area in a terrain unit follows a log-Gaussian distribution, which is the same assumption we will make in this manuscript. The difference resides in our extension of the same framework to the space-time domain. To do so, we fitted a space-time Log-Gaussian GAM by using the ‘mgcv’ R-package (Wood, 2011). Notably, our GAM formulation can be denoted as follows:

$$\begin{aligned} &\log(A_L) \sim \mathcal{N}(\mu, \sigma^2), \\ &g(\mu) = \alpha + \sum_{i=1}^{m} S_i(x_i) + \sum_{j=1}^{n} \beta_j^{litho} x_j + S(lon, lat) + S(time) \end{aligned} \tag{1}$$

where A_L is the cumulative landslide planimetric area in each slope unit, u and σ^2 are the mean and variance of the Gaussian distribution respectively, g is the log link, α is the global intercept, S_i are the smooth functions associated with a number of nonlinear covariates x_i (all covariates except lithology and spatial effect), β_j^{litho} is the regression coefficient for the lithology class x_j, $S(lon, lat)$ denotes the interaction smooth of longitude and latitude to account for the spatial structure. $S(time)$ represents the smooth function associated with the temporal effect between subsequent landslide occurrences.

On a final note, the 119,545 SUs analyzed here do not represent the whole space-time domain expressed across the 14 examined years and the whole landscape of Taiwan. They are rather a subset of it, corresponding to the positive part of the landslide size distribution. Because of this, we stress here that our modeling protocol will make us to use the fitted model to extent the prediction for the remaining 525,491 SUs. We are aware that these SUs do not undergo any landsliding but we opted to graphically simulated over those units to get a full picture, albeit overestimated, of the expected landslide size distribution over the whole space-time domain.

3.3. Model evaluation

Below we describe the metrics and schemes to evaluate the model performance both in terms of goodness-of-fit and predictive performance. In both cases, three numerical metrics are considered namely, mean absolute error (MAE), root mean square error (RMSE), and Pearson correlation coefficient (R). We recall here that we only used 119,545 SUs with mapped landslides for landslide size modelling. For the goodness-of-fit, we fitted an explanatory model with 100% of the dataset and interpreted the effects of covariates. Aside from above numerical metrics, we used three common graphical methods to assess the goodness-of-fit (Wood, 2006), namely, plot of observed versus fitted values, QQ plot, and histogram of residuals.

We used the above three numerical metrics and the plot of observed versus predicted values to evaluate the predictive performance. Moreover, four different cross-validation schemes were implemented for validation, namely, random 10-fold cross-validation (10fold-CV), spatial leave-one-out cross-validation (S-CV), temporal leave-one-out cross-validation (T-CV), and spatio-temporal leave-one-out cross-validation (ST-CV). The 10fold-CV is the most common and conservative scheme to assess model performance. It randomly splits the original dataset into 10 equal-sized subsets and repeatedly fits the model with nine subsets and validates with the one left-out. The S-CV scheme first divides the whole dataset into 12 spatial subsets by considering the administrative partitioning of Taiwan, and then repeatedly leaves out one of the twelve subsets for validation and fits the model with the remaining subsets. Similar to S-CV, the T-CV is based on 14 temporal subsets and validated year by year. As for the ST-CV, it generates 168 subsets based on above 12 spatial partitioning and 14 time intervals, and then executes the leave-one-out validation procedure. For better description the validation schemes, **Fig. 2** show the validation schemes used in this study (except 10-

fold-CV).

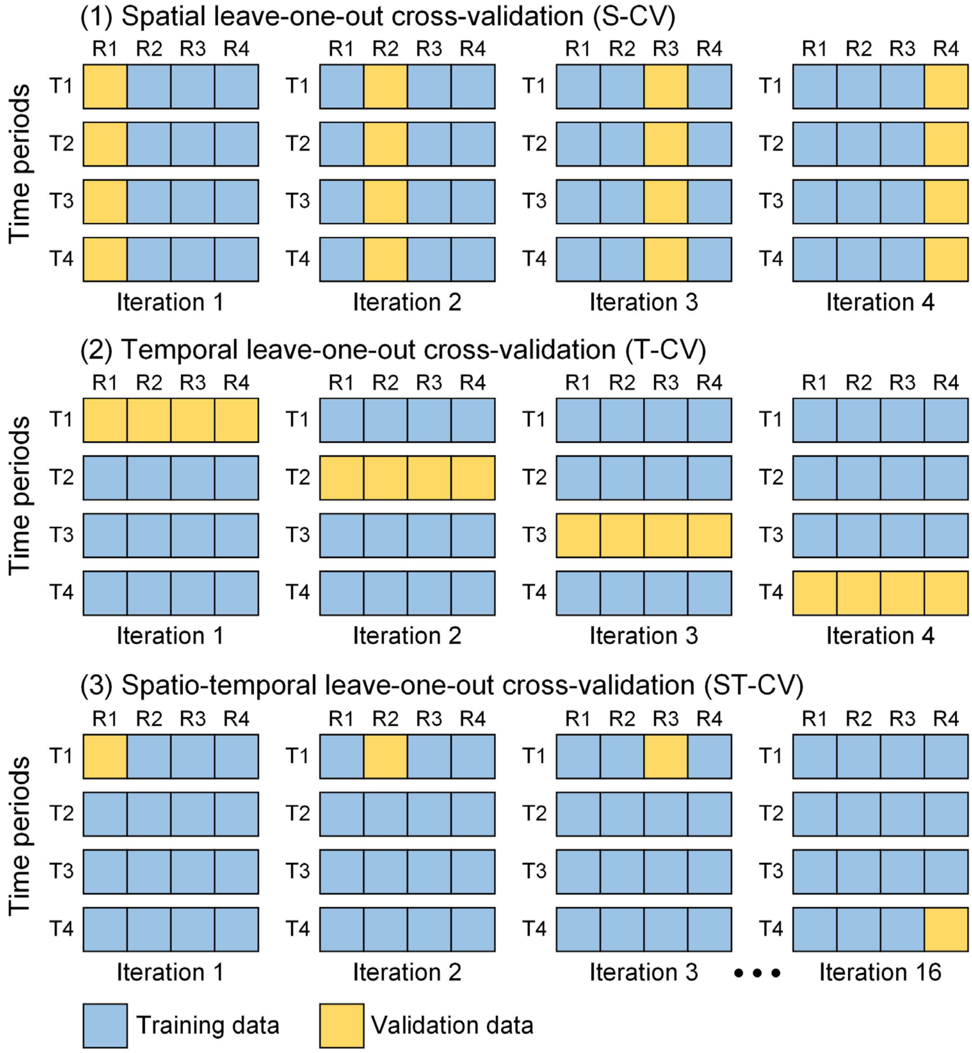

Fig. 2 spatial, temporal, and spatio-temporal cross-validation schemes. Assuming that the study area contains 4 spatial regions and 4 time periods. The row in the figure means data in different time periods, and the column denotes the data in different spatial sub-regions. Therefore, the entire dataset can be divided into 16 small parts.

4. Results

4.1. Model construction and goodness-of-fit

In the modelling process, we first implemented a forward-stepwise procedure to assess whether a given covariate would provide effective information for landslide size modelling. This covariate selection procedure relies on the Akaike information criterion (AIC; Akaike, 1974), where a lower AIC value is diagnostic of a better model.

Specifically, we first ran all single-covariate models, from which we selected the covariate with the lowest AIC value. Then, we focused on selecting the best two-covariate model, then three-covariate one and so on, each time choosing the combination that has led to the minimum AIC. This process stopped when the decrease in AIC value fell below a threshold of 100. **Table 2** shows the overview of the forward-stepwise procedure described above. The final covariate set includes slope unit area, NDVI-SD, maximum daily rainfall, Mean NDVI, time periods, coordinate of slope units, mean profile curvature, mean slope, Slope-SD, mean eastness, lithology, ReliefVar-SD, and mean plan curvature.

Table 2 Results of the forward-stepwise covariate selection

Step	Selected covariate	AIC	Improvement
1	Slope unit area	346734	/
2	NDVI-SD	317164	29570
3	Maximum daily rainfall	308237	8927
4	Mean NDVI	302228	6009
5	Time periods	297896	4332
6	Coordinate of slope units	296051	1845
7	Mean profile curvature	294976	1075
8	Mean slope	293829	1147
9	Slope-SD	293121	708
10	Mean eastness	292443	678
11	Lithology	292141	302
12	ReliefVar-SD	291894	247
13	Mean plan curvature	291722	172
14	Mean northness	291657	65

This covariate set was used as the basis to construct an explanatory space-time model. **Fig. 3** shows an overview of the goodness-of-fit via three criteria, namely, observed versus fitted values, QQ plot, and histogram of residuals (all in log-scale). Inspection of **Fig. 3 (a)** shows that the model achieves a high degree of agreement between the observed and fitted landslide areas per slope unit. The QQ plot presents deviance residuals against theoretical quantiles of the deviance residuals distribution (Wood, 2006). In **Fig. 3 (b)** and **(c)**, we observe that the QQ plot is close to a straight line and the histogram of residuals is consistent with normality, indicating an excellent fitting performance. In addition, we also calculated the statistical criteria for fitting evaluation, that is, the MAE, RMSE, and R is 0.657, 0.817, and 0.673, respectively. Overall, our model thus shows a satisfying goodness-of-fit.

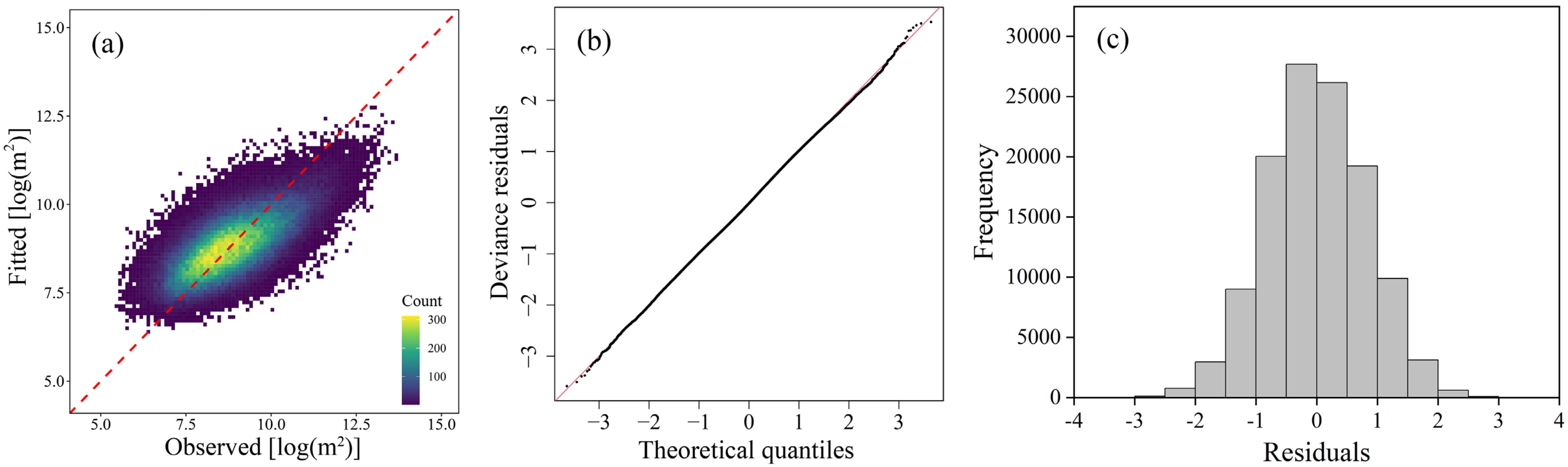

Fig. 3 Goodness-of-fit of the model: (a) observed versus fitted plot (in log-scale), (b) QQ plot and (c) histogram of residuals.

4.2. Covariates' effect

The effects of all covariates with estimated 95% confidence intervals are shown in **Fig. 4**. Slope steepness, with a narrow confidence interval, has a positive effect on landslide size above 26º. Plan curvature and profile curvature show similar nonlinear effects on landslide size estimation, and maintain negative effects above 0.02 and 0.03, respectively. The effect of eastness indicates that slope units facing east are expected to have large landslide areas. Although we allowed the regression coefficients of all covariates to vary nonlinearly, the Slope-SD shows a linear effect on landslide size. We considered this as the best way to represent the effect of Slope-SD optimized by the smoothness selection procedure. The ReliefVar-SD has a positive effect on landslide size when the value is above 609. For the SU-Area, it maintains a negative effect on landslide size until the value reaches 5.6 km^2.

Rainfall is a key dynamic factor related to landslide occurrences. In our study, the maximum daily rainfall for each time period was selected for modelling. Inspection of **Fig. 4** shows that the maximum daily rainfall has very narrow confidence intervals and presents a positive effect with rainfall above 420 mm per day. And, the regression coefficient increases with the daily maximum rainfall. For the dynamic factor of NDVI, the mean NDVI maintains a positive effect on landslide size until 0.67, and then the regression coefficient decreases with the NDVI value. The NDVI-SD has a significant and positive effect on landslide size from 0.09 to 0.23. For the lithology covariate, 11 classes show significant and positive effects on landslide area estimation. Specifically, the class F (Mudstone intercalated with allochthonous material) has the highest positive effect, followed by the class N (Shale, siltstone, and sandstone) and class J (Sandstone, mudstone, and shale).

We recall here that we considered the temporal and spatial effects in the landslide size modelling through a function of time and a function that expresses the interaction of latitude and longitude, respectively. In **Fig. 4**, we observe that the temporal function shows a marked oscillation, with a “wavelength” of about 8 years. For the spatial effect (**Fig. 5**), some clusters emerged in certain regions. For example, the central and northeast parts show negative effects on landslide size, whereas the southwest and northwest fringe parts present positive effects.

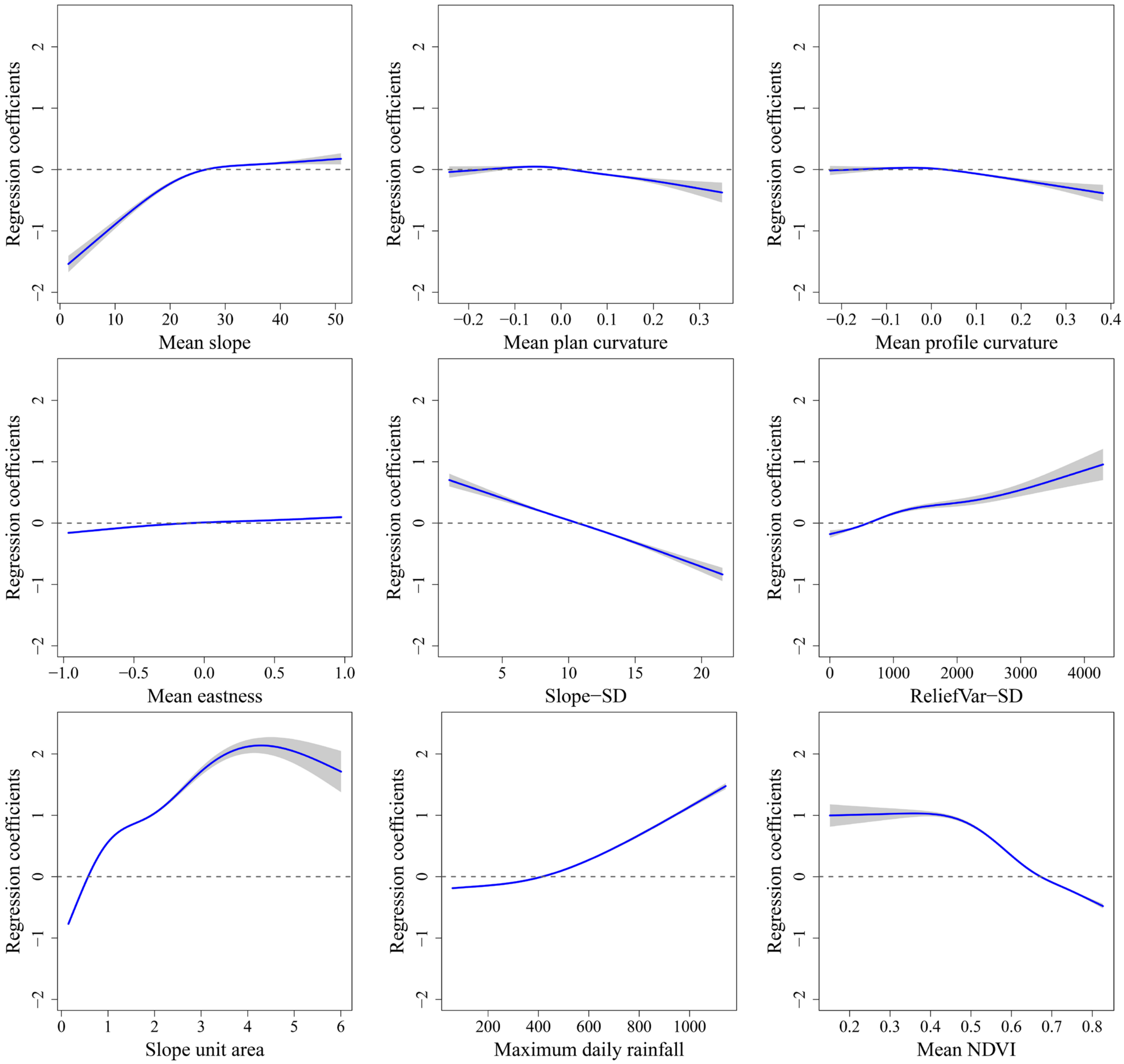

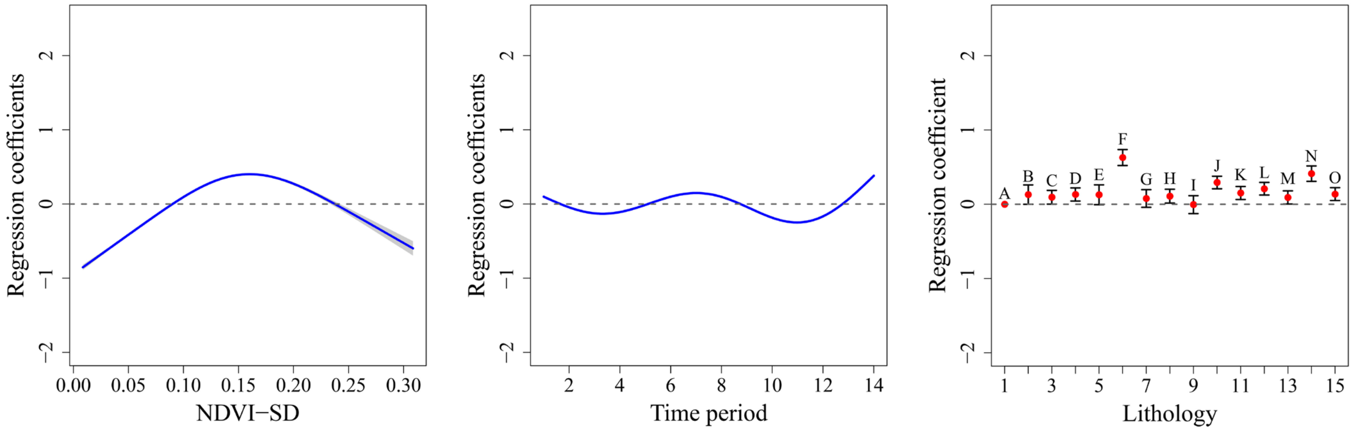

Fig. 4. Summary of effects of covariates. For lithology, the red dots show the regression coefficient, and the vertical segments are the 95% confidence intervals. For other nonlinear effects, the blue curves show the regression coefficient and the shadowed polygons denotes the 95% confidence intervals.

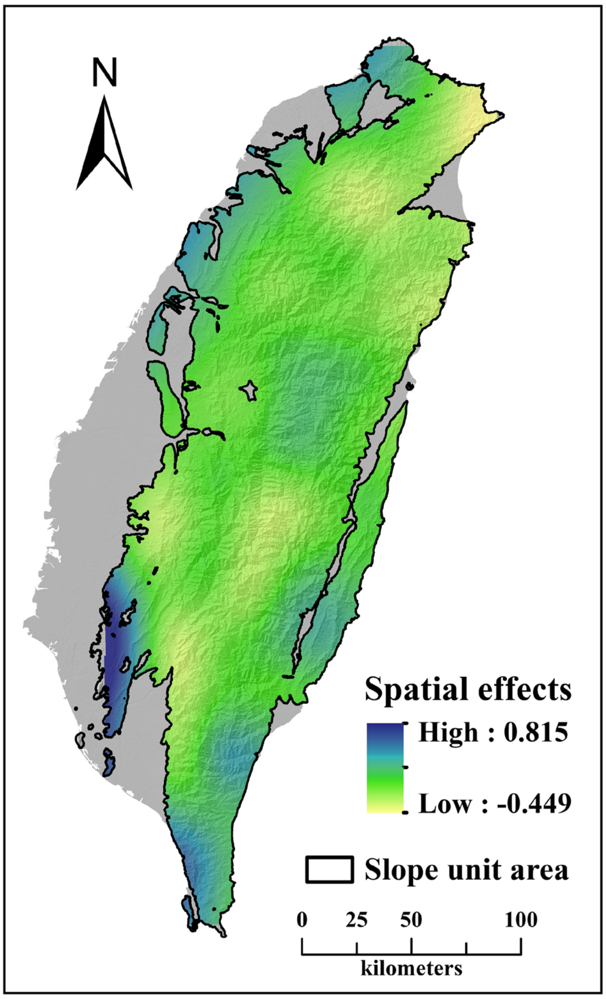

Fig. 5. Spatial effect in the space-time model

4.3. Space-time predictive performance

Aside from the goodness-of-fit assessment, it is also important to test whether the model predicts well on "unknown" samples distributed both in space and time. Thus, we performed a suite of CV procedures to assess the predictive performance of the proposed model in different perspectives, namely, 10fold-CV, S-CV, T-CV, and ST-CV. Note that the space division for S-CV and ST-CV is based on the administrative unit of Taiwan, as shown in **Fig. 6**, and the description of different sub-regions is given to Appendix B. To maintain a comparable number of samples in each sub-region, we merged some small counties or cities.

The predictive performance of 10fold-CV, S-CV, and T-CV is presented in **Fig. 7**, measured via MAE, RMSE, and Pearson correlation coefficient (R). We observe that the 10fold-CV achieves the most stable results among the three CV schemes and its three evaluation indices do not vary significantly. This is because the 10fold-CV randomly selects validation samples from the whole space-time domain, thus limiting the spatial and temporal perturbation induced with respect to the original data distribution. Thus, we extended our validation scheme to incorporate S-CV and T-CV procedures. In **Fig. 7**, the T-CV shows larger metric fluctuations compared to S-CV, indicating that the temporal perturbation to the data distribution is more prominent than the spatial one, although our space-time model still returns good performance. To further investigate the predictive ability of our model across different time periods or geographical regions, we summarize the relative variations in performance in **Fig. 8**. There, we observe that the MAE and RMSE show similar fluctuations in the two CV procedures. This may be because both indices represent the error between the observed and predicted landslide areas. As for the R index, the S-CV returns the highest value while predicting over the sub-region 5, and achieves relatively low values of less than 0.6 while predicting over sub-regions 1 and 2. For the T-CV procedure, the model has the highest R value in T6, and the lowest in T5.

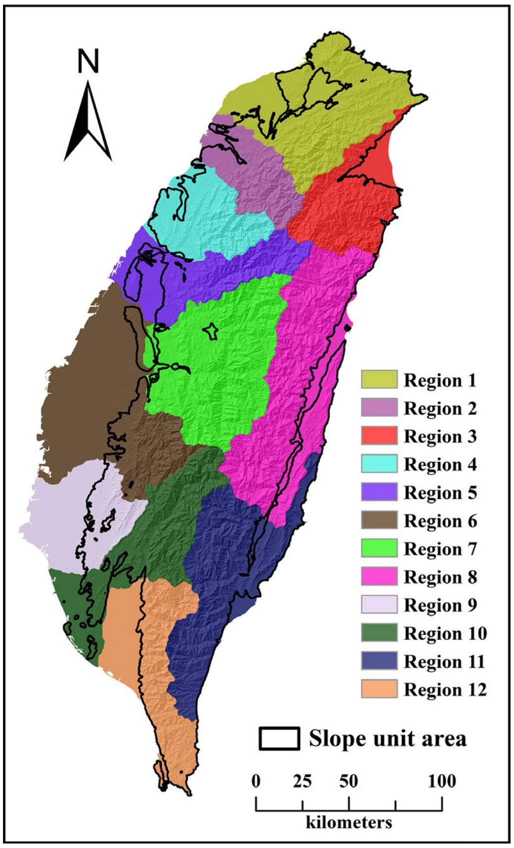

Fig. 6. Spatial sub-regions for validation.

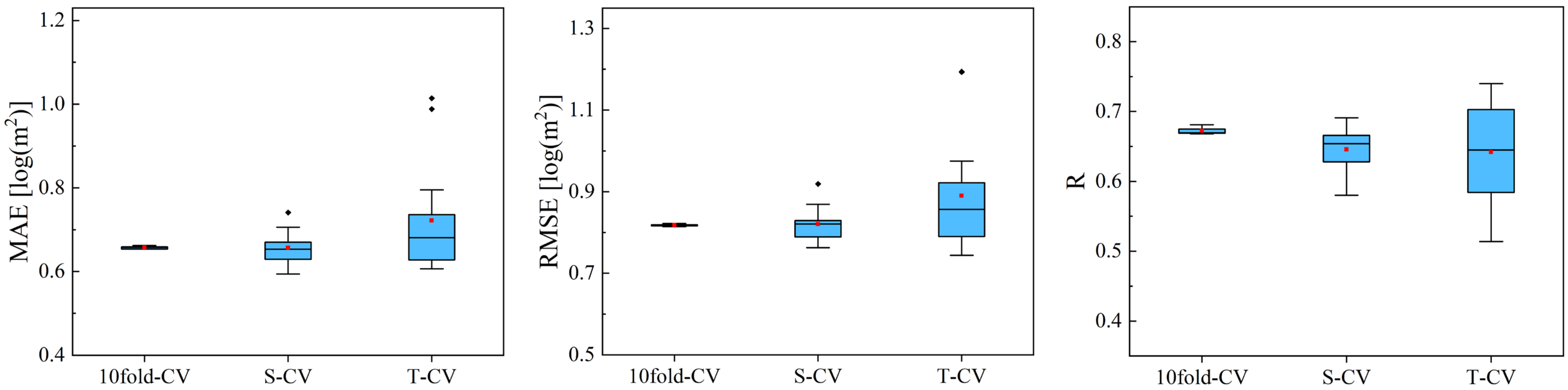

Fig. 7. Predictive performance of 10fold-CV, S-CV, and T-CV

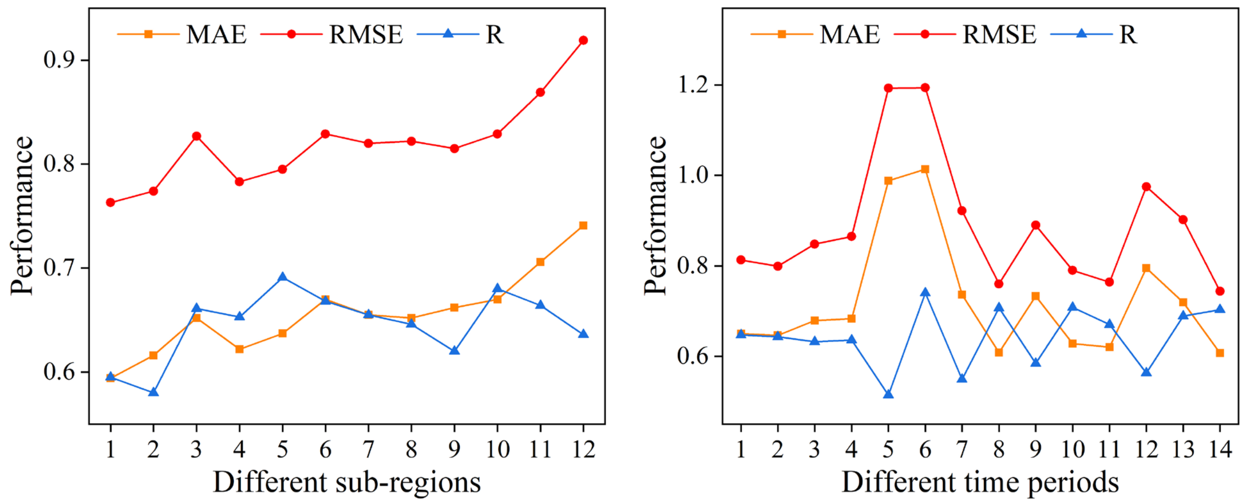

Fig. 8. Performance variations of different sub-regions and time periods.

Finally, we implemented a ST-CV procedure to contextually assess the size predictive performance in both spatial and temporal dimensions. We recall here that we divided the whole space-time domain into 168 parts with 12 spatial and 14 time intervals, and samples in each part were validated separately. **Fig. 9** shows the predictive performance of the ST-CV scheme. Note that each boxplot denotes the temporal variation in a given spatial sub-region. We observe that the model achieves a good prediction performance with mean MAE, RMSE, and R values of 0.661, 0.817, and 0.646, respectively. Inspection of the boxplots shows that three evaluation indexes have greater fluctuations in northern (sub-region 1 and 2) and southern (sub-region 11 and 12) parts of Taiwan than other sub-regions. Moreover, we can observe that the ST-CV scheme results in higher performance variations than 10-fold CV, S-CV, and T-CV, because this validation procedure exaggerates both spatial and temporal difference.

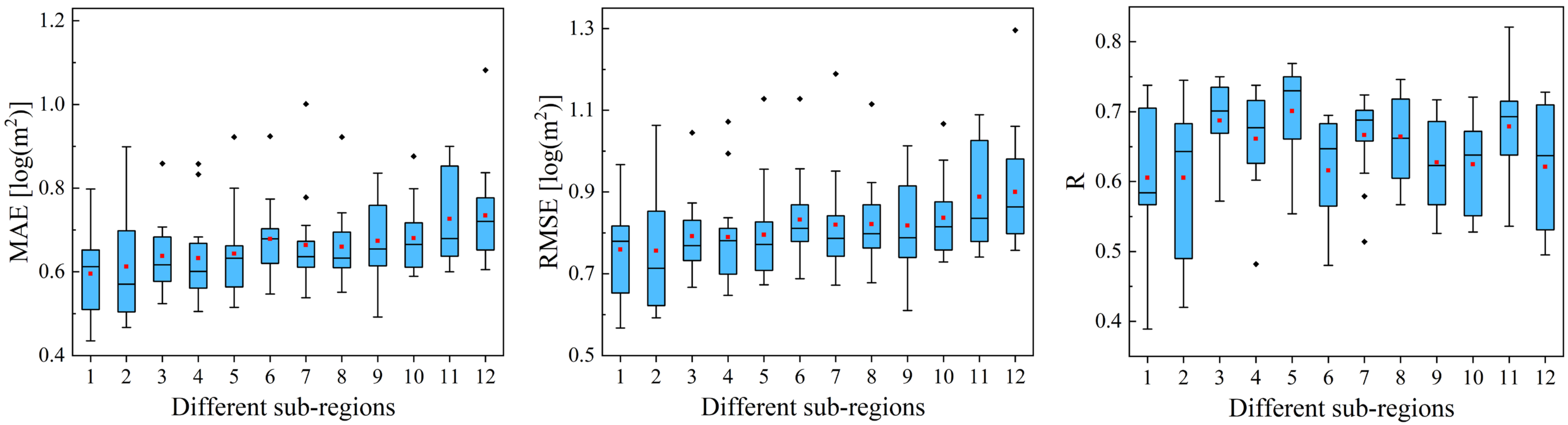

Fig. 9. Predictive performance of ST-CV

We also provide scatter plots to show the visual agreement between observed and predicted landslide areas for different CV schemes (**Fig. 11**). One can see how well the predicted values agrees with the actual ones, for they roughly aligned with the 45° line. Inspection of **Fig. 11** shows that all models achieve reasonable predictive performance, and the 10fold-CV, S-CV, and ST-CV presents slightly better aligned spread along the 45° line than T-CV. Moreover, four models exhibit slightly overestimations in the left tail and underestimations in the right tail.

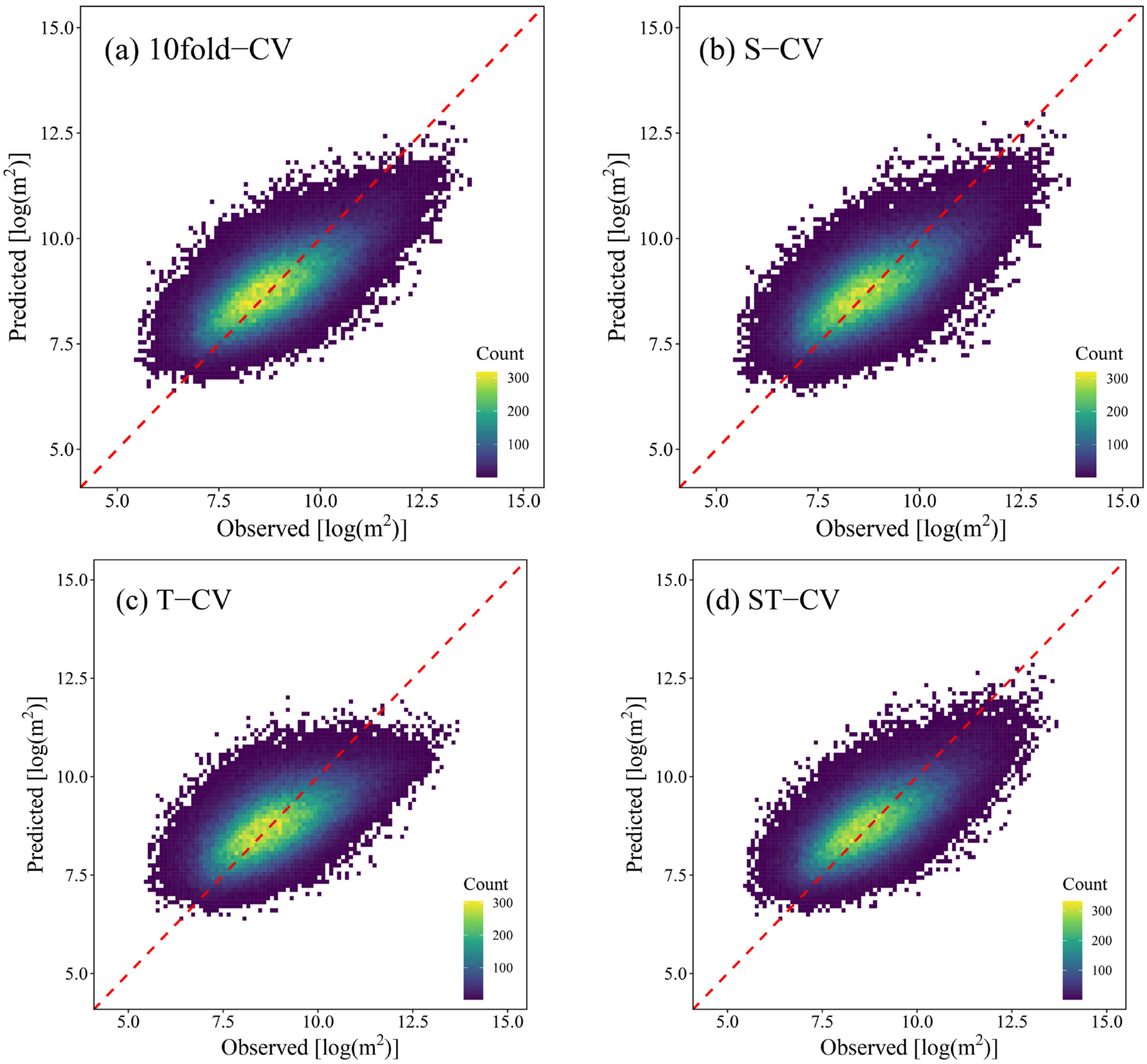

Fig. 10. Observed versus fitted plots (in log-scale) for different CV schemes.

4.4. Landslide size mapping

We used the T-CV procedure to predict the landslide size maps of the 14 time periods, as shown in **Fig. 11**. We also present the plot of predicted versus observed areas for each landslide size predictive map. We can observe that the 14 landslide size maps have strong spatial variations over time. A cluster of larger landslide areas can be seen in southern Taiwan, appearing in T6 (2009-2010), peaking at T7 (2010-2011), then gradually disappearing. Inspection of these scatter plots shows that the model obviously overestimates the landslide size in T5 (2008-2009), T9 (2012-2013), and T12 (2015-2016), and underestimates the landslide size in T6 (2009-2010), T10 (2013-2014), and T13 (2016-2017). Although the model predicts well and produces values aligned with the along the 45° line in other years, a slight overestimation in the left tails, and underestimation in the right tails can be observed.

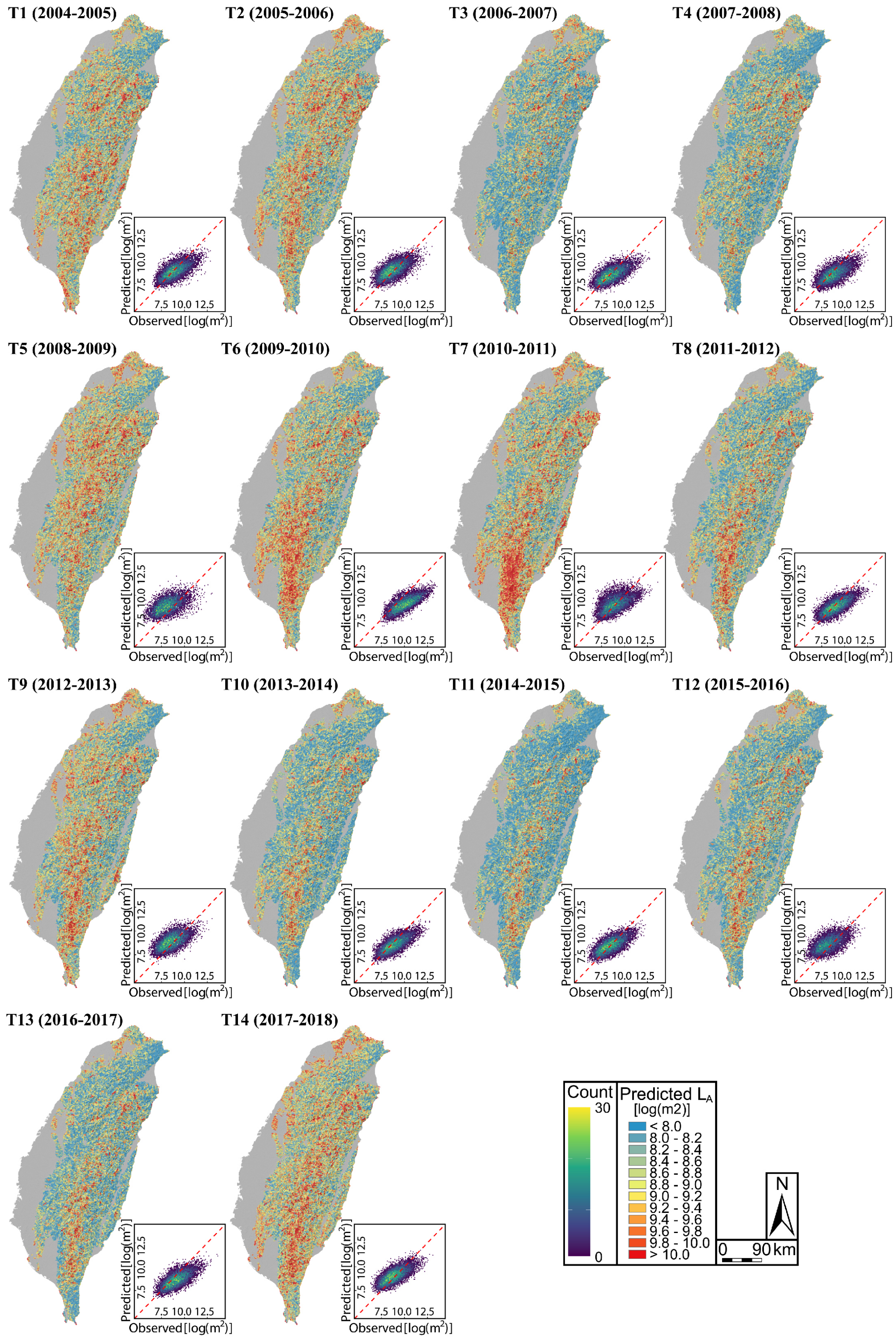

Fig. 11. Landslide size predictive maps in Taiwan from 2004 to 2018. Scatter plots shows the predictive versus observed landslide areas for each time period.

5. Discussion

5.1. Model performance

Our space-time-size model goes beyond the traditional susceptibility model to estimate the landslide planimetric areas across within SUs, and extend the spatially-explicit size model (Lombardo et al., 2021) into both spatial and temporal dimensions. Our explanatory model achieves a satisfying goodness-of-fit (**Fig. 3**) and is able to portray the effects of covariates in an interpretable manner (**Fig. 4**). Moreover, it is important to measure the predictive performance of the size model. Lombardo et al. (2021) implemented a general spatial validation, and Moreno et al. (2022) then extended it into a spatially explicit validation to evaluate the spatial transferability of the model across specific regions. However, as our model is contextually constructed over space and time, we need to explore the predictive ability across the whole space-time domain. We presented a full suite of cross-validation routines from the spatial, temporal, and spatio-temporal standpoints (see Section 3.3). Overall, the predictive performance estimated via different validation schemes achieves good results confirmed through numerical metrics (**Fig. 7** and **Fig. 9**) and graphical methods (**Fig. 10**). We stress here that another improvement in cross-validation process is the implementation of ST-CV. This can be viewed a complete spatio-temporal validation scheme capable of exploring the prediction ability of landslide size models over any time period and in any geographic location.

However, there are still some limitations or some aspects can be further improved. First, the landslide area is expressed on a logarithmic scale and is then assumed to follow a Gaussian distribution. Note that this logarithmic transformation is commonly used in landslide magnitude studies (Guzzetti et al., 2002; Malamud et al., 2004; Medwedeff et al., 2020). Although the logarithm function is monotonous increasing, the landslide area on such scale is hard to interpret for practical usage. On the other hand, converting the prediction results from logarithmic scale into actual expression (m^2) would exacerbate the difference in very low or very large areas (Lombardo et al., 2021). This is likely the result of the Gaussian likelihood choice, which struggles to predict well the behavior in the tail of a skewed distribution. This also stands out in our model results, where we can always observe a slight overestimation in the left tail and a slight underestimation in the right tail. This is valid not only in the predictions of all space-time domain (**Fig. 10**), but also when we look at specific temporal predictions (**Fig. 11**). We thus envision future efforts to test a more suitable probability distribution for space-time landslide size modelling. Second, the space-time domain in our size model is constrained by present and past situations. It lacks an actual prediction for specific future time period. We envision this to be improved by simulating future scenarios of dynamic factors, following a simulation approach analogous to the scheme proposed by Lombardo and Tanyas (2021), in the context of earthquake scenarios for landslide susceptibility.

5.2. Interpretation of covariates

A good model should not only maintain high performance, but also need to be interpretable. Here, we discuss the effects of covariates on space-time size modelling from a geomorphological or statistical perspective (see **Fig. 4**). The terrain slope shows a monotone trend with the regression coefficient, indicating that steeper landscapes are expected to generate larger mass movements. This observation is consistent with Katz et al. (2014) who performed numerical simulations to study the controls on landslide size. The authors concluded that the detachment of material from steeper slopes largely disintegrates while propagating downhill, thus covering a larger planimetric area upon arrest. The plan curvature and profile curvature negligibly contribute to explaining the landslide size approximately up to 0, and the two covariates show negative effects on landslide size from the threshold onward. This may be because landslide materials are difficult to converge into the sidewardly convex terrain, and the erosion may not prevail in upwardly concave terrain (Ohlmacher, 2007). Furthermore, some studies found that east-facing slopes have a high correlation with landslide occurrences in Taiwan region (Lee, 2013; Chen et al., 2019a), we extended this relationship into landslide size in this study. As for Slope-SD, this can be considered a proxy to represent the topographical roughness across a give SU. It shows a completely linear effect with landslide size and its effect decreases as the SD value increase. This may be because the SU with a low standard deviation of slope has a smooth and homogeneous landscape, and a large amount of materials will mobilize once the landslide occurs. Or an alternative explanation may have to do with rock mass strength. In fact, strong materials tend to produce rougher landscapes, i.e., large steepness variations. Conversely, softer or unconsolidated material can loosely drape over the bedrock, giving raise to large failures. In this study, we also selected the relief variance (ReliefVar-SD) to describe the variability of elevation information in a circle, because a higher locations intrinsically have a larger gravitational potential energy to be converted into landslide kinematics and thus into overall planimetric extent (Lombardo et al., 2021). This initial hypothesis is confirmed in the ReliefVar-SD plot, where this parameter positively contributes to the increase of landslide sizes. The slope unit area shows a negative effect on very small SUs, while the contribution appears to positive on larger SUs, which is associated with previous study (Bryce et al., 2022). For lithology, the class F (Mudstone intercalated with allochthonous material) has the highest positive effect on landslide size. The Class F often coincides with badland landscapes in Taiwan, which are prone to landsliding, debris flows, and fluvial erosion (Yang et al., 2021). The class N (Shale, siltstone, and sandstone) and class J (Sandstone, mudstone, and shale) also show positive effects on landslide size, which is agreement with the observations of Wu and Chen (2009), as the sandstone, shale and mudstone have been attributed by the authors with the highest landslide rates in central Taiwan.

Upon completing this overview of the contribution of static covariates, below we will summarize how the dynamic ones entered the landslide size estimation. In our study, we used the maximum daily rainfall to express the climatic control over landslide sizes. We observe that the regression coefficient increases with the rainfall, with the maximum daily rainfall contribution becoming positive for values greater than 420 mm per day. Further studies in lines with the considerations above could open up discussion on rainfall thresholds models useful beyond the pure landslide occurrence case (Segoni et al., 2018; Monsieurs et al., 2019; Wang et al., 2021) and towards the size one instead.

NDVI was also used dynamically in time to reflect the effect of the surface vegetation condition. In **Fig. 4**, NDVI clearly maintains a positive effect on landslide size for low values and transitions to a negative regression coefficient for values above 0.67. This is reasonable because high vegetation cover could increase shallow soil shear strength and reduce erosion (Schwarz et al., 2010). As for the NDVI-SD, its contribution appears to be negative for low variation of NDVI within a SU. This effect turns positive for medium variations of the NDVI and goes back to negative for large variations within a SU. This is a complex behavior to interpret, but one explanation could be that a low NDVI-SD value indicates that the vegetation coverage in the SU is uniform, and this situation is likely to occur in SUs that are almost fully covered by vegetation or bare land. Conversely, a SU with high NDVI-SD value may denote a complex and heterogeneous landscape environment, whose contribution to the landslide size may be less straightforward to explain.

Aside from above environmental covariates, our model also considered the temporal and spatial relationship between SUs with different landslide areas. Specifically, we introduced an additional covariate, i.e., each SU was assigned a time period ID. We found that the temporal covariate shows significant oscillations. The two adjacent highest positive effects or lowest negative effects are separated approximately 8 years apart. This could indicate a return period for landslide size variation in time, or being diagnostic of a larger periodic effect due to harsher climatic conditions to which Taiwan may have been exposed in the past. As for the spatial effect, we considered the interaction between longitude and latitude to account for the spatial structure between SUs. In other words, this effect constrains close SU to behave more similarly as compared to SU that are far apart, in relation to the expected landslide size. In turn this can lead to clusters of landslide size, which the spatial effect is denoted in specific regions of Taiwan.

5.3. Hazard considerations

The definition of landslide hazard initially from Varnes (1984), and then improved by Guzzetti et al. (2005), dividing the probability assessment into three components of spatial probability (susceptibility), temporal probability, and size probability. Landslide susceptibility has been successfully estimated based on different methods (Reichenbach et al., 2018; Merghadi et al., 2020). In recent years, two components of spatial and temporal aspects are simultaneously modelled in landslide prediction studies. For example, Lombardo et al. (2020) is the first to build a Bayesian version of Poisson space-time GAM for landslide occurrences. They went beyond traditional susceptibility models to perform space-time estimation of the landslide counts. Wang et al. (2022) tested a space-time binomial generalized linear model for the susceptibility of hydro-morphological process across China. However, the above space-time models neglect the landslide size, which is otherwise accounted for in this work. As a result, by estimating the planimetric area of mass movements per SUs in time we fulfill two components of the hazard definition. We therefore consider this improvement a step towards a next generation model where different aspects of the hazard definition will be estimated jointly.

6. Conclusions

We implemented a space-time size model in the main island of Taiwan from 2004 to 2018. The model corresponding to a Log-Gaussian GAM is capable of estimating landslide planimetric areas per slope unit across the whole space-time domain. We validated the predictive performance of the model based on a complete suite of cross-validation routines by considering spatial, temporal, and spatio-temporal perspectives. The results indicate that the space-time characteristics of landslide size can be captured from stationary and dynamic factors, as well as the relationships between slope units that are close in space and time. This is a significant improvement that goes beyond the traditional susceptibility modelling to perform space-time estimation of landslide size. Moreover, this model is also an extension of space-time susceptibility model, which provide a promising step towards an operational use of landslide size estimation. However, our model does not fully satisfy the definition of hazard as it lacks the information on whether a slope is actually stable or unstable. For this reason, we envision our future efforts to be dedicated to a combinatory model where all requirements of the landslide hazard definition will be addressed in a single analytical protocol. If so, this could further provide the basis for an operational space-time risk model, where the expected loss due to landslides can be probabilistically simulated before reaching the emergency phase. Before reaching this stage though, another potential improvement to be explored could be finding a more suitable probability distribution to reduce the misestimates in the tails. Or even better, we envision to directly model the landslide size in square meters instead of using a logarithmic transformation. Overall, we expect our space-time size prediction model to place a new brick in the landslide literature upon which laying the foundation for future advances in data-driven applications. This new data-driven prototype better portrays the overall landslide information across a given the landscape, and in the hope of triggering similar experiments in the geoscientific community.

Acknowledgement

This work was supported by the Joint Funds of the National Natural Science Foundation of China (U21A2013), the National Natural Science Foundation of China (61271408), the China Scholarship Council (No. 202106410043), and the Fundamental Research Funds for National Universities, China University of Geosciences (Wuhan). This article was also partially supported by King Abdullah University of Science and Technology (KAUST) in Thuwal, Saudi Arabia, Grant URF/1/4338-01-01. We also thank the scientists of Taiwan that made the input data freely available, and would like to thank the handling editor and two anonymous reviewers for their valuable comments and suggestions, which significantly improved the quality of this paper.

Data and codes availability statement

The data and codes that support the findings of this study can be accessed at: https://doi.org/10.5281/zenodo.7005158.

Appendix A. Summary of lithology class

Class	Description
A	Alluvium
B	Andesite, basalt, and serpentine
C	Metamorphic limestone
D	Black schist, green schist, and sandy schist
E	Laterite, gravel, sand and clay
F	Mudstone intercalated with allochthon

G	Gneiss
H	Hard shale and sandstone
I	Agglomerate and tuffaceous sandstone
J	Sandstone, mudstone, and shale
K	Phyllite, slate, and sandstone
L	Sandstone, shale, and coaly shale
M	Quartzite, slate, and coaly shale
N	Shale, siltstone, and sandstone
O	Hard shale, slate, and Phyllite

Appendix B. Description of different sub-regions

Sub-region ID	Description
1	New Taipei City, Taipei City, Keelung City, Taoyuan County
2	Hsinchu City, Hsinchu County
3	Yilan County
4	Miaoli County
5	Taichung City
6	Chiayi County, Chiayi City, Yunlin County, Changhua County
7	Nantou County
8	Hualien County
9	Tainan City
10	Kaohsiung City
11	Taitung County
12	Pingtung County

References

Aguilera, Q., Lombardo, L., Tanyas, H., Lipani, A.: On the prediction of landslide occurrences and sizes via Hierarchical Neural Networks, Stoch. Env. Res. Risk. A., https://doi.org/10.1007/s00477-022-02215-0, 2022.

Akaike, H.: A new look at the statistical model identification, Ieee. T. Automat. Contr, 19, 716-723, 1974.

Alvioli, M. et al.: Automatic delineation of geomorphological slope units with r. slopeunits v1. 0 and their optimization for landslide susceptibility modeling, Geoscientific Model Development, 9, 3975, 2016.

Atkinson, P.M., Massari, R.: Generalised linear modelling of susceptibility to landsliding in the central Apennines, Italy, Comput. Geosci., 24, 373-385, 1998.

Bryce, E., Lombardo, L., van Westen, C., Tanyas, H., Castro-Camilo, D.: Unified landslide hazard assessment using hurdle models: a case study in the Island of Dominica, Stoch. Env. Res. Risk. A., 1-14, 2022.

Cama, M., Lombardo, L., Conoscenti, C., Rotigliano, E.: Improving transferability strategies for debris flow susceptibility assessment: Application to the Saponara and Itala catchments (Messina, Italy), Geomorphology, 288, 52-65, 2017.

Carrara, A., 1988. Drainage and Divide Networks Derived from High-Fidelity Digital Terrain Models. in: Chung, C.F., Fabbri, A.G., Sinding-Larsen, R. (Eds.), Quantitative Analysis of Mineral and Energy Resources. Springer Netherlands, Dordrecht, pp. 581-597.

Chang, C.H., Harrison, J.F., Huang, Y.C.: Modeling Typhoon-Induced Alterations on River Sediment Transport and Turbidity Based on Dynamic Landslide Inventories: Gaoping River Basin, Taiwan, Water, 7, 6910-6930, 2015.

Chang, K.-T., Merghadi, A., Yunus, A.P., Pham, B.T., Dou, J.: Evaluating scale effects of topographic variables in landslide susceptibility models using GIS-based machine learning techniques, Scientific Reports, 9, 12296, 10.1038/s41598-019-48773-2, 2019.

Chen, C.-W. et al.: Assessing landslide characteristics in a changing climate in northern Taiwan, Catena, 175, 263-277, https://doi.org/10.1016/j.catena.2018.12.023, 2019a.

Chen, T.-H.K., Prishchepov, A.V., Fensholt, R., Sabel, C.E.: Detecting and monitoring long-term landslides in urbanized areas with nighttime light data and multi-seasonal Landsat imagery across Taiwan from 1998 to 2017, Remote Sens. Environ., 225, 317-327, 2019b.
Chung, C.-J.F., Fabbri, A.G., Westen, C.J.V., 1995. Multivariate regression analysis for landslide hazard zonation, Geographical information systems in assessing natural hazards. Springer, pp. 107-133.
Corominas, J. et al.: Recommendations for the quantitative analysis of landslide risk, Bull. Eng. Geol. Environ., 73, 209-263, 2014.
Emberson, R., Kirschbaum, D.B., Amatya, P., Tanyas, H., Marc, O.: Insights from the topographic characteristics of a large global catalog of rainfall-induced landslide event inventories, Nat. Hazards Earth Syst. Sci., 22, 1129-1149, 10.5194/nhess-22-1129-2022, 2022.
Fang, Z., Wang, Y., Peng, L., Hong, H.: A comparative study of heterogeneous ensemble-learning techniques for landslide susceptibility mapping, Int. J. Geogr. Inf. Sci., 35, 321-347, 10.1080/13658816.2020.1808897, 2021.
Fell, R. et al.: Guidelines for landslide susceptibility, hazard and risk zoning for land use planning, Eng. Geol., 102, 85-98, 2008.
Gariano, S.L., Guzzetti, F.: Landslides in a changing climate, Earth-sci. Rev., 162, 227-252, 2016.
Goetz, J.N., Guthrie, R.H., Brenning, A.: Integrating physical and empirical landslide susceptibility models using generalized additive models, Geomorphology, 129, 376-386, https://doi.org/10.1016/j.geomorph.2011.03.001, 2011.
Guzzetti, F., Carrara, A., Cardinali, M., Reichenbach, P.: Landslide hazard evaluation: a review of current techniques and their application in a multi-scale study, Central Italy, Geomorphology, 31, 181-216, 10.1016/S0169-555X(99)00078-1, 1999.
Guzzetti, F., Malamud, B.D., Turcotte, D.L., Reichenbach, P.: Power-law correlations of landslide areas in central Italy, Earth. Planet. Sc. Lett, 195, 169-183, https://doi.org/10.1016/S0012-821X(01)00589-1, 2002.
Guzzetti, F. et al.: Landslide inventory maps: New tools for an old problem, Earth-sci. Rev., 112, 42-66, 2012.
Guzzetti, F., Reichenbach, P., Cardinali, M., Galli, M., Ardizzone, F.: Probabilistic landslide hazard assessment at the basin scale, Geomorphology, 72, 272-299, 10.1016/j.geomorph.2005.06.002, 2005.
Hung, J.-J.: Chi-Chi earthquake induced landslides in Taiwan, Earthquake Engineering and Engineering Seismology, 2, 25-33, 2000.
Jaiswal, P., van Westen, C.J., Jetten, V.: Quantitative landslide hazard assessment along a transportation corridor in southern India, Eng. Geol., 116, 236-250, https://doi.org/10.1016/j.enggeo.2010.09.005, 2010.
Jones, J.N., Boulton, S.J., Stokes, M., Bennett, G.L., Whitworth, M.R.: 30-year record of Himalaya mass-wasting reveals landscape perturbations by extreme events, Nat. Commun., 12, 1-15, 2021.
Katz, O., Morgan, J.K., Aharonov, E., Dugan, B.: Controls on the size and geometry of landslides: Insights from discrete element numerical simulations, Geomorphology, 220, 104-113, https://doi.org/10.1016/j.geomorph.2014.05.021, 2014.
Lee, C.-T., 2013. Re-evaluation of factors controlling landslides triggered by the 1999 Chi–Chi earthquake, Earthquake-induced landslides. Springer, pp. 213-224.
Lee, C.-T. et al.: Statistical approach to earthquake-induced landslide susceptibility, Eng. Geol., 100, 43-58, https://doi.org/10.1016/j.enggeo.2008.03.004, 2008.
Lin, C.-W. et al.: Landslides triggered by the 7 August 2009 Typhoon Morakot in southern Taiwan, Eng. Geol., 123, 3-12, 2011.
Lin, E., Liu, C., Chang, C., Cheng, I., Ko, M.: Using the formosat-2 high spatial and temporal resolution multispectral image for analysis and interpretation landslide disasters in taiwan, J. Photogramm. Remote Sens, 17, 31-51, 2013.
Lin, S.C., Ke, M.C., Lo, C.M.: Evolution of landslide hotspots in Taiwan, Landslides, 14, 1491-1501, 10.1007/s10346-017-0816-9, 2017.
Liu, C.-C.: Preparing a landslide and shadow inventory map from high-spatial-resolution imagery facilitated by an expert system, Journal of Applied Remote Sensing, 9, 096080, 2015.
Lombardo, L. et al.: Geostatistical modeling to capture seismic-shaking patterns from earthquake-induced landslides, Journal of Geophysical Research: Earth Surface, 124, 1958-1980, 2019.
Lombardo, L., Opitz, T., Ardizzone, F., Guzzetti, F., Huser, R.: Space-time landslide predictive modelling, Earth-sci. Rev., 103318, https://doi.org/10.1016/j.earscirev.2020.103318, 2020.
Lombardo, L., Opitz, T., Huser, R.: Point process-based modeling of multiple debris flow landslides using INLA: an application to the 2009 Messina disaster, Stoch. Env. Res. Risk. A., 32, 2179-2198, 2018.

Lombardo, L., Tanyas, H.: From scenario-based seismic hazard to scenario-based landslide hazard: fast-forwarding to the future via statistical simulations, Stoch. Env. Res. Risk. A., 1-14, 2021.
Lombardo, L., Tanyas, H., Huser, R., Guzzetti, F., Castro-Camilo, D.: Landslide size matters: A new data-driven, spatial prototype, Eng. Geol., 106288, 2021.
Malamud, B.D., Turcotte, D.L., Guzzetti, F., Reichenbach, P.: Landslide inventories and their statistical properties, Earth. Surf. Proc. Land, 29, 687-711, 2004.
Medwedeff, W.G., Clark, M.K., Zekkos, D., West, A.J.: Characteristic landslide distributions: An investigation of landscape controls on landslide size, Earth. Planet. Sc. Lett, 539, 116203, 2020.
Merghadi, A. et al.: Machine learning methods for landslide susceptibility studies: A comparative overview of algorithm performance, Earth-sci. Rev., 2020, 103225, 10.1016/j.earscirev.2020.103225 2020.
Monsieurs, E., Dewitte, O., Demoulin, A.: A susceptibility-based rainfall threshold approach for landslide occurrence, Nat. Hazards Earth Syst. Sci., 19, 775-789, 2019.
Moreno, M., Steger, S., Tanyas, H., Lombardo, L.: Modeling the size of co-seismic landslides via data-driven models: the Kaikōura's example, 2022.
Nandi, A., Shakoor, A.: A GIS-based landslide susceptibility evaluation using bivariate and multivariate statistical analyses, Eng. Geol., 110, 11-20, https://doi.org/10.1016/j.enggeo.2009.10.001, 2010.
Nefeslioglu, H.A., Gorum, T.: The use of landslide hazard maps to determine mitigation priorities in a dam reservoir and its protection area, Land Use Policy, 91, 104363, 2020.
Nowicki Jessee, M.A. et al.: A Global Empirical Model for Near-Real-Time Assessment of Seismically Induced Landslides, Journal of Geophysical Research: Earth Surface, 123, 1835-1859, https://doi.org/10.1029/2017JF004494, 2018.
Ohlmacher, G.C.: Plan curvature and landslide probability in regions dominated by earth flows and earth slides, Eng. Geol., 91, 117-134, https://doi.org/10.1016/j.enggeo.2007.01.005, 2007.
Opitz, T., Bakka, H., Huser, R., Lombardo, L.: High-resolution Bayesian mapping of landslide hazard with unobserved trigger event, The Annals of Applied Statistics, 16, 1653-1675, 2022.
Park, J.-Y., Lee, S.-R., Lee, D.-H., Kim, Y.-T., Lee, J.-S.: A regional-scale landslide early warning methodology applying statistical and physically based approaches in sequence, Eng. Geol., 260, 105193, https://doi.org/10.1016/j.enggeo.2019.105193, 2019.
Reichenbach, P., Rossi, M., Malamud, B., Mihir, M., Guzzetti, F.: A review of statistically-based landslide susceptibility models, Earth-sci. Rev., 180, 60-91, 10.1016/j.earscirev.2018.03.001, 2018.
Rossi, M. et al.: A predictive model of societal landslide risk in Italy, Earth-sci. Rev., 196, 102849, 2019.
Schwarz, M., Preti, F., Giadrossich, F., Lehmann, P., Or, D.: Quantifying the role of vegetation in slope stability: A case study in Tuscany (Italy), Ecol. Eng., 36, 285-291, 2010.
Segoni, S., Piciullo, L., Gariano, S.L.: A review of the recent literature on rainfall thresholds for landslide occurrence, Landslides, 15, 1483-1501, 2018.
Steger, S., Brenning, A., Bell, R., Glade, T.: The influence of systematically incomplete shallow landslide inventories on statistical susceptibility models and suggestions for improvements, Landslides, 14, 1767-1781, 2017.
Steger, S., Brenning, A., Bell, R., Petschko, H., Glade, T.: Exploring discrepancies between quantitative validation results and the geomorphic plausibility of statistical landslide susceptibility maps, Geomorphology, 262, 8-23, 10.1016/j.geomorph.2016.03.015, 2016.
Stepinski, T.F., Jasiewicz, J.: Geomorphons-a new approach to classification of landforms, Proceedings of geomorphometry, 2011, 109-112, 2011.
Tanyaş, H., Allstadt, K.E., van Westen, C.J.: An updated method for estimating landslide-event magnitude, Earth. Surf. Proc. Land, 43, 1836-1847, https://doi.org/10.1002/esp.4359, 2018.
Tanyaş, H., Hill, K., Mahoney, L., Fadel, I., Lombardo, L.: The world's second-largest, recorded landslide event: Lessons learnt from the landslides triggered during and after the 2018 Mw 7.5 Papua New Guinea earthquake, Eng. Geol., 297, 106504, 2022.
Titti, G., van Westen, C., Borgatti, L., Pasuto, A., Lombardo, L.: When Enough Is Really Enough? On the Minimum Number of Landslides to Build Reliable Susceptibility Models, Geosciences, 11, 469, 2021.
Van den Bout, B., Lombardo, L., Chiyang, M., van Westen, C., Jetten, V.: Physically-based catchment-scale prediction of slope failure volume and geometry, Eng. Geol., 284, 105942, 2021.
Van Westen, C., Rengers, N., Soeters, R.: Use of geomorphological information in indirect landslide susceptibility assessment, Nat. Hazards, 30, 399-419, 2003.
Varnes, D.J., 1984. Landslide hazard zonation: a review of principles and practice. UNESCO Press, Paris, 63 pp.
Wang, N. et al.: Space-time susceptibility modeling of hydro-morphological processes at the Chinese

national scale, Eng. Geol., 301, 106586, https://doi.org/10.1016/j.enggeo.2022.106586, 2022.
Wang, N. et al.: Using satellite rainfall products to assess the triggering conditions for hydro-morphological processes in different geomorphological settings in China, International Journal of Applied Earth Observation and Geoinformation, 102, 102350, 2021.
Wood, S.N., 2006. Generalized additive models: an introduction with R. chapman and hall/CRC.
Wood, S.N.: Fast stable restricted maximum likelihood and marginal likelihood estimation of semiparametric generalized linear models, Journal of the Royal Statistical Society: Series B (Statistical Methodology), 73, 3-36, 2011.
Wu, C.-H., Chen, S.-C.: Determining landslide susceptibility in Central Taiwan from rainfall and six site factors using the analytical hierarchy process method, Geomorphology, 112, 190-204, 10.1016/j.geomorph.2009.06.002, 2009.
Yang, C.-J., Turowski, J.M., Hovius, N., Lin, J.-C., Chang, K.-J.: Badland landscape response to individual geomorphic events, Nat. Commun., 12, 4631, 10.1038/s41467-021-24903-1, 2021.
Zhang, J. et al.: How size and trigger matter: analyzing rainfall-and earthquake-triggered landslide inventories and their causal relation in the Koshi River basin, central Himalaya, Nat. Hazards Earth Syst. Sci., 19, 1789-1805, 2019.